



# Graphite functionalization by ball milling with sulfur

Aniello Vittore<sup>1</sup> · Maria Rosaria Acocella<sup>1</sup> · Gaetano Guerra<sup>1</sup> 

© Springer Nature Switzerland AG 2019

## Abstract

The present study reports on ball-milling of high-surface-area graphite in the presence of sulfur, mainly considering high graphite/sulfur (G/S) weight ratios. Graphitic crystallites after co-milling with sulfur maintain essentially unaltered crystalline order while exhibit heavily functionalized lateral edges, mainly by O=S=O and S=O groups. Solvent extraction procedures and thermogravimetric experiments show that co-milled graphite/sulfur samples contain two different kinds of sulfur: an extractable one being only physically adsorbed on graphite (exhibiting a higher thermal stability) and a non-extractable fraction chemically bonded to defective graphitic sites (exhibiting a lower thermal stability). The amount of sulfur covalently bonded to graphite crystallites increases with the co-milling time up to a limit value, which is in the range 3.0–3.5 wt% and is poorly dependent on the starting G/S ratio.

**Keywords** X-ray diffraction · Edge functionalization · Thermogravimetric analysis · Solvent extraction

## 1 Introduction

For many graphite and graphene applications, mainly for those needing high electrical conductivity, the presence of ordered graphitic structure with functional groups being confined to the graphitic edges, is often preferred [1–6].

Graphite functionalization by ball-milling of graphite with gases (CO<sub>2</sub>, N<sub>2</sub>, F<sub>2</sub> and Cl<sub>2</sub>), liquids (SO<sub>3</sub>, Br<sub>2</sub>) and solids (I<sub>2</sub>, maleic anhydride and elemental sulfur) have been described by many reports. These low-cost procedures are environmentally sustainable and can also lead to selective functionalization of graphite edges by different functional groups [2, 7–13].

In particular, by ball-milling of graphite in the presence of sulfur it was demonstrated that sulfur could edge-selectively functionalize graphene nanoplatelets with a concomitant homogeneous adsorption on and within the graphitic crystallites [14, 15]. These literature studies have been conducted by using excess of sulfur with respect to

graphite, (maximum G/S ratio equal to 1) and showed that only a low fraction of sulfur is covalently bonded to graphite while most of sulfur is simply adsorbed by graphite, even for long term milling [14, 15].

Graphene nanoplatelets edge-functionalized with sulfur have been proposed as highly efficient lithium-sulfur batteries cathode materials [14, 15] and could be in principle suitable as reinforcing and reactive agents for polymer composites.

The aim of the present study is to explore the possibility to achieve graphite functionalization by using much smaller amounts of sulfur and to establish a simple method to discriminate between bound and adsorbed sulfur.

**Electronic supplementary material** The online version of this article (<https://doi.org/10.1007/s42452-019-0179-z>) contains supplementary material, which is available to authorized users.

✉ Gaetano Guerra, [gguerra@unisa.it](mailto:gguerra@unisa.it) | <sup>1</sup>Department of Chemistry and Biology and INSTM Research Unit, Università di Salerno, Fisciano, SA, Italy.



SN Applied Sciences (2019) 1:169 | <https://doi.org/10.1007/s42452-019-0179-z>

Received: 30 November 2018 / Accepted: 14 January 2019 / Published online: 18 January 2019

## 2 Experimental section

High surface area graphite, exhibiting a surface area of 330 m<sup>2</sup>/g, was obtained from Asbury Graphite Mills Inc.

Ball-milling was conducted by a “FRITSCHE Pulverisette 7 Premium Line” with spinning rate of 400 rpm.

Sulfur extraction was conducted by treatment with liquid chloroform followed by powder desiccation at 60 °C.

Wide-angle X-ray diffraction (WAXD) patterns were collected by an automatic Bruker D2 Phaser diffractometer, in reflection, at 35 kV and 40 mA, using the nickel filtered Cu-K $\alpha$  radiation (1.5418 Å). Correlation lengths relative to different hkl crystalline reflections ( $D_{hkl}$ ) were determined by using Scherrer's equation:

$$D_{hkl} = \frac{K\lambda}{\beta_{hkl} \cos \theta_{hkl}} \quad (1)$$

where  $\lambda$  is the wavelength of the incident X-rays and  $\theta_{hkl}$  and  $\beta_{hkl}$  are the diffraction angle and the full width at half maximum (FWHM) of the reflections, respectively. The Scherrer's constant  $K$  was assumed equal to 1.

Thermogravimetric analyses (TGA) were conducted by a TA-Instruments Q500, under nitrogen flow of 50 mL/min, with a heating rate of 10 °C/min, up to 800 °C.

FTIR spectra were obtained with a FTIR (BRUKER Vertex70) spectrometer equipped with deuterated triglycine sulfate (DTGS) detector and a KBr beam splitter, at a resolution of 2.0 cm<sup>-1</sup>. The frequency scale was internally calibrated to 0.01 cm<sup>-1</sup> using a He-Ne laser. 32 scans were signal averaged to reduce the noise. Spectra of powder samples were collected by using potassium bromide (KBr) pellets.

Differential Scanning Calorimetry (DSC) scans were collected by a DSC Q2000 provided by (TA instruments).

Surface areas of carbon and oxidized carbon samples were measured by nitrogen adsorption at liquid nitrogen temperature (77 K) with a Nova Quantachrome 4200e instrument. Before adsorption measurements, samples were degassed at 60 °C under vacuum for 24 h. The surface area ( $SA_{BET}$ ) values were determined by using 11-point BET analysis.

Elemental analysis was performed with a Thermo FlashEA 1112 Series CHNS-O analyzer, after pre-treating samples in an oven at 100 °C for 12 h, by using BBOT as standard.

## 3 Results and discussion

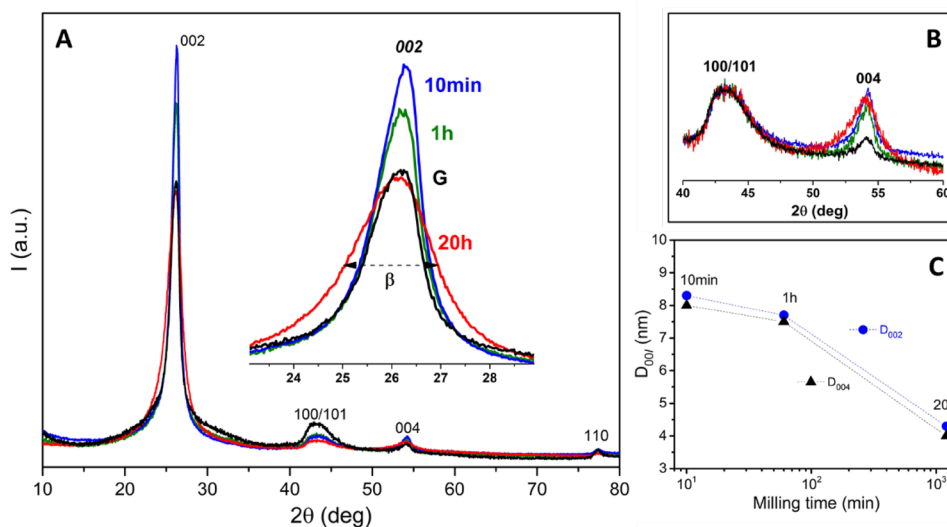
The first two sections of this paper are devoted to ball-milling procedures on as received graphite and sulfur samples. The subsequent section deals with co-milling of graphite and sulfur, by considering mixtures with prevailing content of graphite.

### 3.1 Milling of graphite

The high surface area graphite ( $SA_{BET} = 330$  m<sup>2</sup>/g) used for our study presents the WAXD pattern shown by a black curve in Fig. 1. The ill-defined 101 peak indicates disorder in the relative position of parallel graphitic layers, i.e. the occurrence of a structure close the disordered turbostratic one [16, 17]. Moreover, the FWHM of the reflections allows evaluating crystal correlation lengths being higher in the graphitic planes ( $D_{110} \approx 30$  nm) than perpendicular to the graphitic planes ( $D_{002} \approx 10$  nm) [17].

After short-term milling (e.g., after 10 min, blue curves in Fig. 1A, B) 002 and 004 reflections, corresponding to crystal planes parallel to the graphitic planes, become

**Fig. 1** **A, B** WAXD (CuK $\alpha$ ) patterns of a high surface area graphite before and after different milling times. **A** Patterns normalized on the overall diffraction area in the range 12°–80°. **B** Patterns enlarged in the  $2\theta$  range 40°–60° and normalized on the area of the broad peak at 41° <  $2\theta$  < 46°. **C** Correlation lengths of 002 and 004 reflections versus milling time



definitely more intense than for the starting graphite (black curves in Fig. 1A, B). This result can be rationalized by considering that short term milling induces an orientation of graphite platelets that is preferentially parallel to the plane of the sample holder of the diffractometer. This orientation leads to an apparent increase of intensities of 00 *l* reflections, as collected by an automatic powder diffractometer.

The FWHM of 002 (Fig. 1A) and 004 (Fig. 1B) reflections increase with milling time and correspondingly a remarkable reduction of the correlation length perpendicular to the graphitic planes, down to 4 nm, is evaluated (Fig. 1C). This indicates that long term milling leads to a significant graphite delamination.

As already known [7, 8, 18, 19], ball milling of graphite also leads to its oxidation. Quantitative evaluation of the oxygen content has been effected by elemental analysis. As shown in the last column of Table 1, O/C weight ratio increases up to 0.02 and 0.07 after 1 h and 20 h of milling, respectively.

Informative on the milling process are also surface area values, as evaluated by BET measurements (2nd column of Table 1). After 1 h of milling there is only a small reduction of SA from 330 m<sup>2</sup>/g down to nearly 300 m<sup>2</sup>/g. For long term milling (20 h), the surface area becomes lower than 10 m<sup>2</sup>/g. This phenomenon is possibly due to agglomeration of nanostructured particles, as already known for ball milling of graphite [20].

The remarkable oxidation of graphite is also clearly pointed out by FTIR measurements, like those shown in Fig. 2A. In fact, as the milling time increases, a progressive increase of broad bands in the 1250–1000 cm<sup>-1</sup> region, typical of vibrational modes of C–O bonds, is observed. This indicates the formation of different oxygenated functional groups, mainly hydroxyl and epoxide.

The formation of a significant amount of oxygenated groups definitely reduces thermal stability of graphite. This is shown for instance by TGA scans, like those shown in Fig. 2B. It is apparent that 10 min of milling (blue scan) do not change the thermal stability of graphite (black scan) while the decrease of thermal stability is remarkable after 20 h of milling. Moreover, the increase of weight loss below 100 °C with long term ball-milling (Fig. 2B) clearly indicates increase of hydrophilicity.

### 3.2 Milling of sulfur

Sulfur used for this study presents the WAXD pattern shown by a black curve in Fig. 3A, which exhibits typical crystal reflections of the orthorhombic phase [21, 22]. After 20 h of milling, although a broad amorphous halo appears, a large fraction of the sample maintains an ordered orthorhombic crystalline structure.

DSC scans of the untreated sulfur sample (black curve in Fig. 3B) show two endothermic phenomena: a lower one at 107 °C with  $\Delta H_t \approx 12$  J/g, corresponding to the orthorhombic  $\rightarrow$  monoclinic transition [23, 24] and a higher one at

**Table 1** Surface area and elemental analysis of graphite after different milling times

Milling times (h)	SA <sub>BET</sub> (m <sup>2</sup> /g)	%N	%C	%H	%O	O/C
1	297	0.60	97.6	0.12	1.6	0.02
20	7	0.54	92.3	0.34	6.8	0.07

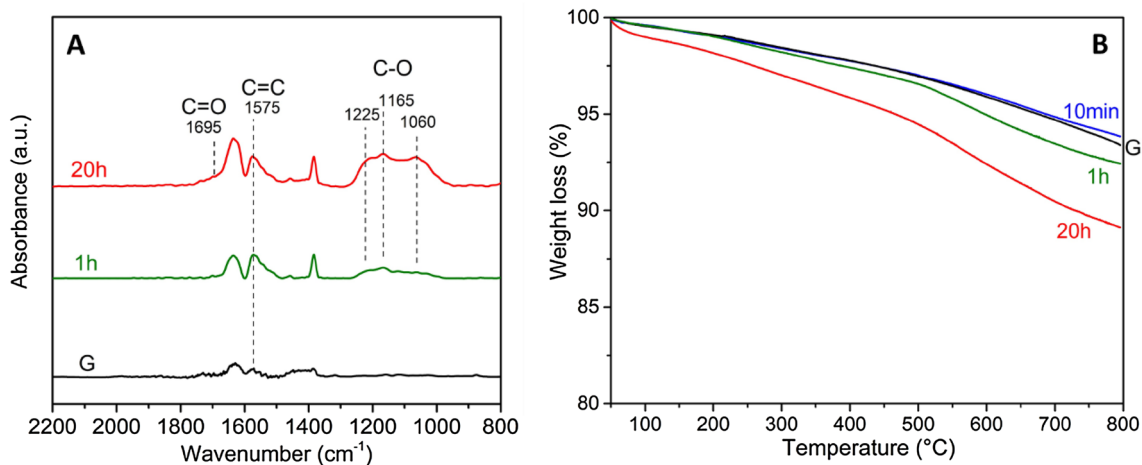


**Fig. 2** FTIR (A) and TGA (B) measurements on the graphite, before and after ball milling for 10 min, 1 h and 20 h

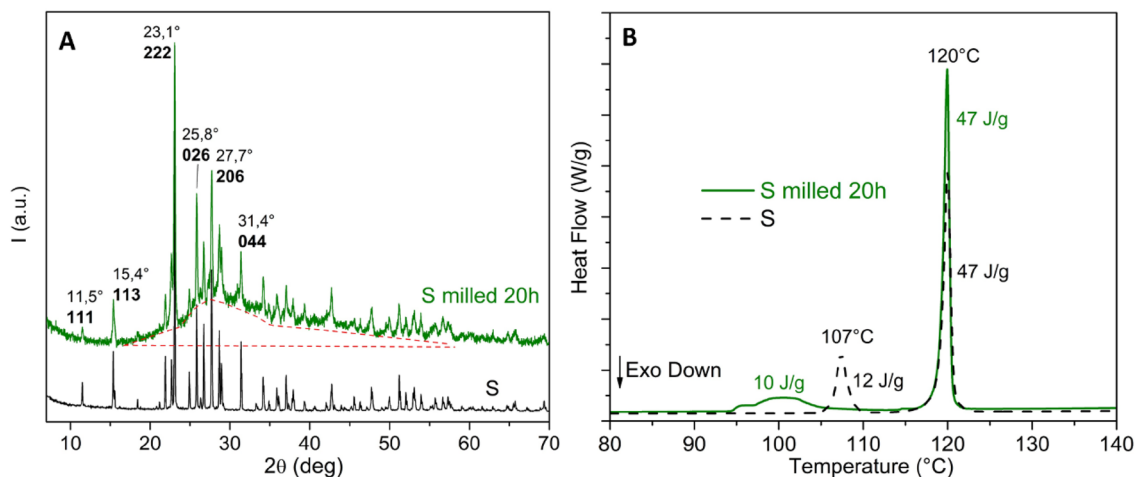


**Fig. 3** WAXD (CuKα) patterns (A) and DSC scans at 10 °C/min (B) of sulfur before and after ball milling for 20 h

120 °C with  $\Delta H_m \approx 47$  J/g, corresponding to the melting of the monoclinic phase. A DSC scan of the sulfur sample after 20 h of milling (green curve in Fig. 3B) again shows two well-separated endothermic phenomena, but the lower peak becomes much broader and centered at lower temperature (100 °C), with only slightly reduced transition enthalpy ( $\Delta H_t \approx 10$  J/g).

This confirms that long term ball milling reduces the crystalline order of the orthorhombic phase thus reducing the temperature of the orthorhombic  $\rightarrow$  monoclinic transition. The unaltered melting enthalpy ( $\Delta H_m \approx 47$  J/g) clearly indicates that the long-term ball milling does not produce chemical modification of sulfur.

### 3.3 Co-milling of graphite and sulfur

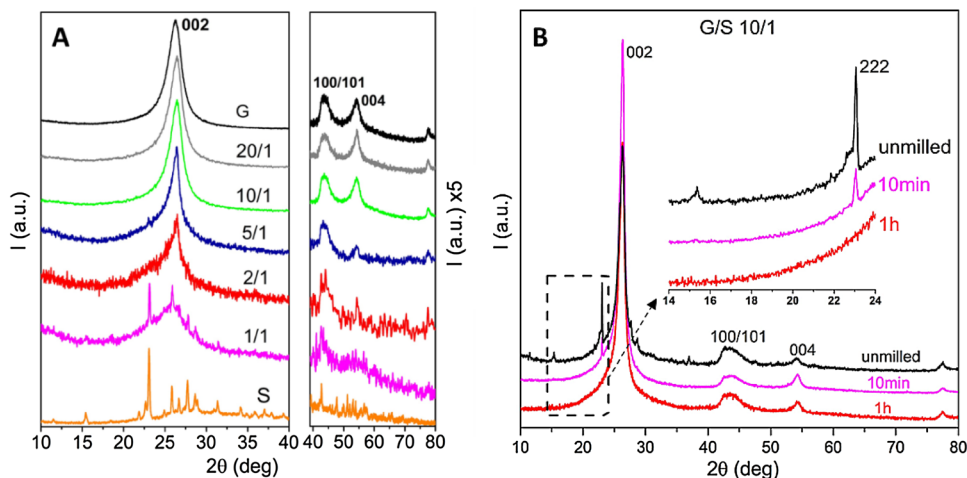
WAXD (CuKα) patterns of graphite (upper black curve), sulfur (lower orange curve) and of different graphite/sulfur (G/S) wt/wt mixtures, after 20 h of ball-milling are

shown in Fig. 4A. It is apparent that the orthorhombic crystallinity of sulfur, after 20 h of co-milling disappears, for  $G/S \geq 2/1$ .

WAXD patterns of samples milled for shorter times and  $G/S = 10/1$  are shown in Fig. 4B. It is apparent that already after 10 min of co-milling crystalline peaks of sulfur have nearly completely disappeared (only a weak 222 reflection, at  $2\theta \approx 23^\circ$ , is still detectable, purple pattern in Fig. 4B). Also, this latter reflection disappears after 1 h of co-milling (red pattern in Fig. 4B).

The effect of co-milling with sulfur on the crystalline structure of graphite is nearly negligible for  $G/S \geq 10/1$  (upper patterns of Fig. 4A). As the sulfur content increases, the 002 peak corresponding to the interlayer graphitic distance, becomes broader and broader. For  $G/S = 1/1$ , after removal of the crystalline sulfur by extraction by chloroform, the correlation length perpendicular to the graphitic planes, as evaluated by the Sherrer method decreases from  $\approx 10$  nm to  $\approx 3$  nm.

**Fig. 4** WAXD (CuKα) patterns of: **A** graphite, sulfur and graphite/sulfur wt/wt mixtures, after ball-milling for 20 h; **B** graphite/sulfur 10/1 mixture, unmilled and after milling times of 10 min or 1 h



Particularly informative on the co-milling products are TGA scans, like those for samples milled for 20 h (Fig. 5A). All the reported scans exhibit a weight loss close to the amount of sulfur used. However, as the sulfur content decreases, there is a substantial shift toward higher temperatures of this weight loss phenomenon. This is also more clearly shown by the plot of temperature of half-weight loss ( $T_{1/2}$ ) versus the sulfur content of Fig. 5C. This phenomenon can be in part explained by a delay of sulfur sublimation due to attractive interactions with the graphitic surface, possibly associated with electronic interactions between sulfur  $3p_z^2$  orbitals and  $\pi$  orbital of graphite [25].

Also informative are differential thermo-gravimetric (DTG) scans. DTG scans of Fig. 5B, corresponding to the TGA scans of Fig. 5A, show the occurrence of two separate weight loss phenomena.

The presence of two separated weight loss phenomena is also more clearly apparent by considering TGA and DTG scans of samples with high G/S ratios, by changing the co-milling time. This is shown for instance for G/S = 20/1, for milling times in the range 1–30 h, in Fig. 6. DTG curves (inset in Fig. 6) show that the lower temperature peak increases at expenses of the higher temperature peak, as the milling time increases.

To understand the origin of the two DTG peaks associated with sulfur loss, co-milled samples have been subjected to different solvent extraction procedures. Gravimetric measurements show that G/S = 20/1 mixtures (S content of 4.8%), co-milled for 20 h and 30 h, present a weight loss after extraction by chloroform of nearly 2% and 1.5%, respectively. Elemental analyses of G/S 20/1 co-milled for 20 h and 30 h, show that the sulfur content in the extracted samples is close to 2.9% and 3.5%, respectively (Table S1 of Supplementary Information), in satisfactory agreement with the weight loss data. Similar contents of bonded sulfur were obtained also for mixtures with much larger sulfur content.

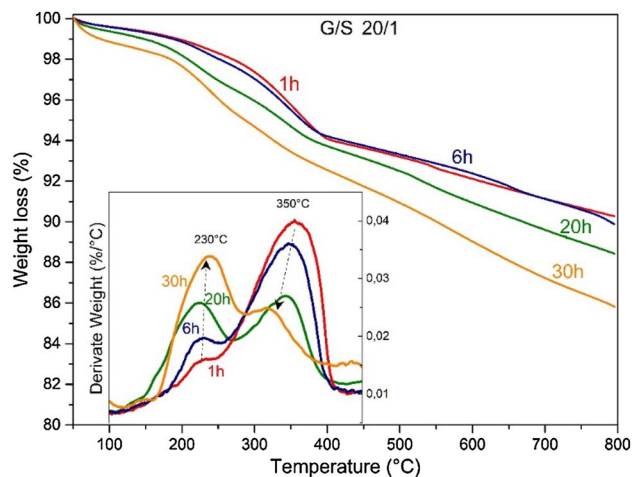


**Fig. 6** TGA scans and DTG scans (inset) of a graphite/sulfur 20/1 mixture, after different milling times. Black arrows in the inset indicate intensity peak variations by increasing milling time

TGA and DTG scans of G/S 20/1 mixtures, as milled for 20 h and 30 h, before and after extraction with chloroform are compared in Fig. 7.

Particularly informative are DTG scans of Fig. 7B, D, showing that the solvent extraction involves essentially only sulfur whose thermal loss occurs at higher temperature (corresponding to the DTG peak centered in the range 325–350 °C). In fact, the lower temperature DTG peak, roughly centered at 230 °C, remains nearly unaltered.

These results can be easily rationalized by assuming that the higher temperature weight losses of Figs. 6 and 7 correspond to sulfur absorbed on graphene surfaces while the lower temperature weight losses correspond to degradation of covalently bound sulfur. The amount of covalently bound sulfur, possibly located on edges of graphitic planes, increases by increasing ball milling time (Fig. 6).

FTIR spectra of the graphite sample and of the G/S mixtures, after milling for 20 h, are shown in Fig. 8A, for

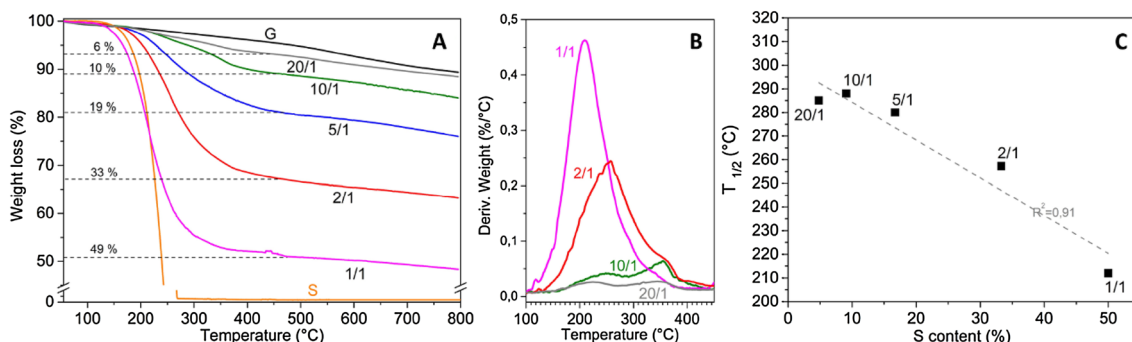


**Fig. 5** TGA (A) and DTG (B) scans of graphite, sulfur and of graphite/sulfur wt/wt mixtures, after 20 h of ball-milling. C Plot of temperature of half-weight loss ( $T_{1/2}$ ) versus sulfur content. Close to curves and experimental points, graphite/sulfur wt/wt ratios are indicated

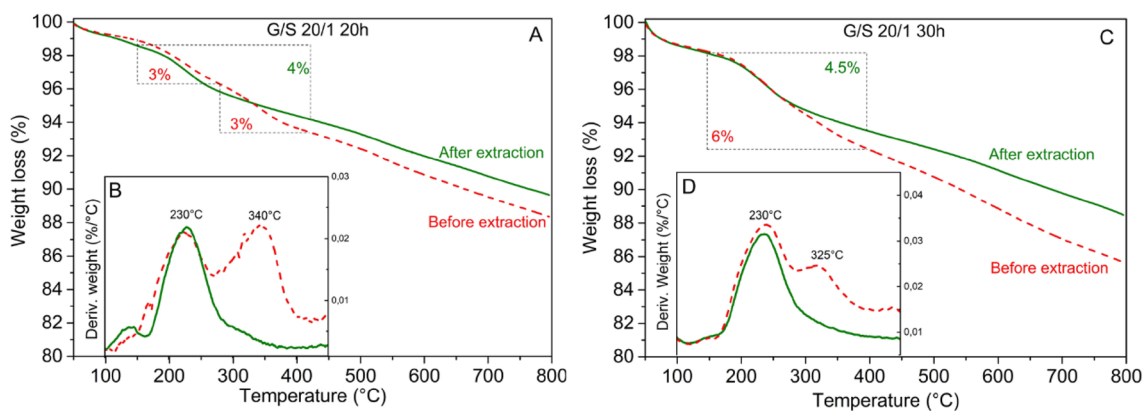


**Fig. 7** TGA (**A, C**) and DTG (**B, D**) scans of a graphite/sulfur, 20/1 mixture, after 20 h (**A, B**) and 30 h (**C, D**) of milling, before (red dashed line) and after (green solid line) partial sulfur extraction by chloroform

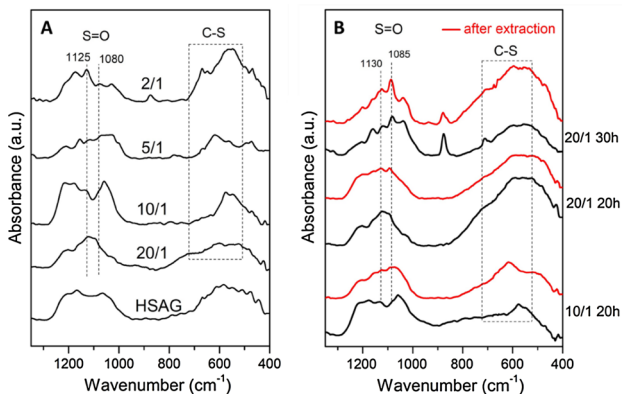


**Fig. 8** FT-IR spectra of ball-milled graphite and G/S wt/wt samples, in the spectral range 1350–400  $\text{cm}^{-1}$ : **A** milling time of 20 h; **B** ball milled for different compositions and times, before (black spectra) and after (red spectra) extraction

the spectral range 1300–400  $\text{cm}^{-1}$ . The ball-milled graphite presents two broad bands in the spectral ranges 1250–1000  $\text{cm}^{-1}$  and 700–450  $\text{cm}^{-1}$ , which are associated with different oxidized groups ( $\text{O}/\text{C} = 0.07$ ) in different graphitic sites. In fact, it is well known that milling of graphite in the presence of air leads to formation of oxidized groups, mainly carbonyl, hydroxyl and epoxides [18, 19].

Although these bands remain broad for co-milled G/S samples, for high sulfur content (upper spectrum of Fig. 8A) and for long term ball milling (upper spectra of Fig. 8B) better defined peaks, centered in the 1130–1125  $\text{cm}^{-1}$  and 1085–1080  $\text{cm}^{-1}$  ranges, possibly associated with stretching of  $\text{O}=\text{S}=\text{O}$  and  $\text{S}=\text{O}$  bonds, respectively, are apparent. It is also possible to exclude the presence of  $\text{S}-\text{H}$  bonds due to the absence of the typical bands in the 2600–2540  $\text{cm}^{-1}$  range [26].

A comparison between FTIR spectra of three co-milled samples before and after chloroform extraction is reported

in Fig. 8B. It is apparent that extraction of absorbed sulfur does not change significantly the observed FTIR spectra.

For a more precise definition of the sulfur containing species, FTIR identification of species released by thermogravimetric measurements could be included in future studies.

## 4 Conclusions

Crystallinity of graphite is poorly affected by ball-milling procedures, with only a reduction below 5 nm of correlation length perpendicular to the graphitic crystallites, for long milling times. This behavior is not changed by co-milling with sulfur. Sulfur, on the contrary, as a consequence of milling with graphite, becomes fully amorphous and time needed to a complete loss of crystal order markedly decreases with the graphite/sulfur weight ratio, becoming of only few minutes for  $\text{G}/\text{S} \geq 20$ .

However, even for G/S ratios as high as 20, relevant functionalization of graphitic edges is achieved, mainly occurring as  $\text{O}=\text{S}=\text{O}$  and  $\text{S}=\text{O}$  groups.

Solvent extraction procedures and thermogravimetric measurements show that co-milled graphite/sulfur samples contain two different kinds of sulfur: (A) an extractable one only physically adsorbed on graphite, exhibiting a higher thermal stability, with DTG peak close to 350 °C; (B) a non-extractable fraction chemically bonded to defective (mainly edge) graphitic sites, exhibiting a lower thermal stability, with DTG peak close to 230 °C.

The amount of sulfur covalently bonded to graphite crystallites increases with the co-milling time up to a limit value, which is in the range 3.0–3.5 wt% with respect to graphitic carbon and is poorly dependent on the used G/S ratio.

Highly crystalline graphite as functionalized by co-milling with sulfur could be considered as reinforcing and reactive filler for polymer composites.

## Compliance with ethical standards

**Conflict of interest** On behalf of all authors, the corresponding author states that there is no conflict of interest.

## References

1. Choi E-K, Jeon I-Y, Oh S-J, Baek J-B (2010) *J Mater Chem* 20:10936–10942
2. Liu K, Chen S, Luo Y, Jia D, Gao H, Hu G, Liu L (2013) Edge-functionalized graphene as reinforcement of epoxy-based conductive composite for electrical interconnects. *Compos Sci Technol* 88:84–91
3. Abdolmaleki A, Mallakpour S, Borandeh S (2014) Structure morphology and electronic properties of L-phenylalanine edge-functionalized graphite platelets through Friedel–Crafts acylation reaction. *RSC Adv* 4:60052–60057
4. Guadagno L, Raimondo M, Vertuccio L, Mauro M, Guerra G, Lafdi K, De Vivo B, Lamberti P, Spinelli G, Tucci V (2015) Optimization of graphene-based materials outperforming host epoxy matrices. *RSC Adv* 5:36969–36978
5. Seo J-M, Baek J-B, Tan L-S (2017) Defect/edge-selective functionalization of carbon materials by direct Friedel–Crafts acylation reaction. *Adv Mater* 29(19):1606317
6. Barbera V, Brambilla L, Porta A, Bongiovanni R, Vitale A, Torrisi G, Galimberti M (2018) Selective edge functionalization of graphene layers with oxygenated groups by means of Reimer–Tiemann and domino Reimer–Tiemann/Cannizzaro reactions. *J Mater Chem A* 6:7749–7761
7. Jeon I-Y, Shin Y-R, Sohn G-J, Choi H-J, Bae S-Y, Mahmood J, Jung S-M, Seo J-M, Kim M-J, Chang DW (2012) Edge-carboxylated graphene nanosheets via ball milling. *Proc Natl Acad Sci USA* 109:5588–5593
8. Jeon I-Y, Choi H-J, Jung S-M, Seo J-M, Kim M-J, Dai L, Baek J-B (2012) Large-scale production of edge-selectively functionalized graphene nanoplatelets via ball milling and their use as metal-free electrocatalysts for oxygen reduction reaction. *J Am Chem Soc* 135:1386–1393
9. Jeon IY, Zhang S, Zhang L, Choi HJ, Seo JM, Xia Z, Dai L, Baek JB (2013) Edge-selectively sulfurized graphene nanoplatelets as efficient metal-free electrocatalysts for oxygen reduction reaction: the electron spin effect. *Adv Mater* 25:6138–6145
10. Baek J-Y, Jeon I-Y, Baek J-B (2014) Edge-iodine/sulfonic acid-functionalized graphene nanoplatelets as efficient electrocatalysts for oxygen reduction reaction. *J Mater Chem A* 2:8690–8695
11. Beckert F, Trenkle S, Thomann R, Muelhaupt R (2014) Mechanochemical route to functionalized graphene and carbon nanofillers for graphene/SBR nanocomposites. *Macromol Mater Eng* 299:1513–1520
12. Jeon I-Y, Bae S-Y, Seo J-M, Baek J-B (2015) Scalable production of edge-functionalized graphene nanoplatelets via mechanochemical ball-milling. *Adv Funct Mater* 25:6961–6975
13. Kabbani MA, Kochat V, Bhowmick S, Soto M, Som A, Krishnadas KR, Woellner CF, Jaques YM, Barrera EV, Asif S et al (2018) Consolidation of functionalized graphene at ambient temperature via mechano-chemistry. *Carbon* 134:491–499
14. Xu J, Shui J, Wang J, Wang M, Liu HK, Dou SX, Baek JB, Dai L (2014) Sulfur–graphene nanostructured cathodes via ball-milling for high-performance lithium–sulfur batteries. *ACS Nano* 8:10920–10930
15. Yan L, Xiao M, Wang S, Han D, Meng Y (2017) Edge sulfurized graphene nanoplatelets via vacuum mechano-chemical reaction for lithium–sulfur batteries. *J Energy Chem* 26:522–529
16. Li ZQ, Lu CJ, Xia ZP, Zhou Y, Luo Z (2007) X-ray diffraction patterns of graphite and turbostratic carbon. *Carbon* 45:1686–1695
17. Mauro M, Cipolletti V, Galimberti M, Longo P, Guerra G (2012) Chemically reduced graphite oxide with improved shape anisotropy. *J Phys Chem C* 116:24809–24813
18. Dash P, Dash T, Rout TK, Sahu AK, Biswal SK, Mishra BK (2016) Preparation of graphene oxide by dry planetary ball milling process from natural graphite. *RSC Adv* 6:12657–12668
19. Mahmoud AED, Stolle A, Stelter M (2018) Sustainable synthesis of high-surface-area graphite oxide via dry ball milling. *ACS Sustain Chem Eng* 6:6358–6369
20. Hermann H, Schubert Th, Gruner W, Mattern N (1997) Structure and chemical reactivity of ball-milled graphite. *Nanostruct Mater* 8:215–229
21. Abrahams SC (1955) The crystal and molecular structure of orthorhombic sulfur. *Acta Crystallogr* 8:661–671
22. Rettig SJ, Trotter J (1987) Refinement of the structure of orthorhombic sulfur  $\alpha$ -S8. *Acta Crystallogr C* 43:2260–2262
23. Currell BR, Williams AJ (1974) Thermal analysis of elemental sulphur. *Thermochim Acta* 9:255–259
24. Černosek Z, Holubova J, Černoskova E, Ruzicka A (2009) Sulfur—a new information on this seemingly well-known element. *J Non Oxide Glasses* 1:38–42
25. Lin T, Tang Y, Wang Y, Bi H, Liu Z, Huang F, Jiang M (2013) Scotch-tape-like exfoliation of graphite assisted with elemental sulfur and graphene–sulfur composites for high-performance lithium–sulfur batteries. *Energy Environ Sci* 6:1283–1290
26. Lin-Vien D, Colthup NB, Fateley WG, Grasselli JG (1991) The handbook of infrared and Raman characteristic frequencies of organic molecules. Elsevier, Amsterdam